



## OPEN ACCESS

EDITED BY  
Congjian Xu,  
Fudan University, China

REVIEWED BY  
Jinwei Qiang,  
Jinshan Hospital, China  
Haiou Liu,  
Fudan University, China

\*CORRESPONDENCE  
Ai Lian Liu  
✉ liuailian@dmu.edu.cn

SPECIALTY SECTION  
This article was submitted to  
Gynecological Oncology,  
a section of the journal  
Frontiers in Oncology

RECEIVED 23 November 2022  
ACCEPTED 05 January 2023  
PUBLISHED 25 January 2023

CITATION  
Meng X, Tian S, Ma C, Lin L, Zhang X,  
Wang J, Song Q and Liu AL (2023) APTw  
combined with mDixon–Quant imaging to  
distinguish the differentiation degree of  
cervical squamous carcinoma.  
*Front. Oncol.* 13:1105867.  
doi: 10.3389/fonc.2023.1105867

COPYRIGHT  
© 2023 Meng, Tian, Ma, Lin, Zhang, Wang,  
Song and Liu. This is an open-access article  
distributed under the terms of the [Creative Commons Attribution License \(CC BY\)](https://creativecommons.org/licenses/by/4.0/). The  
use, distribution or reproduction in other  
forums is permitted, provided the original  
author(s) and the copyright owner(s) are  
credited and that the original publication in  
this journal is cited, in accordance with  
accepted academic practice. No use,  
distribution or reproduction is permitted  
which does not comply with these terms.

# APTw combined with mDixon–Quant imaging to distinguish the differentiation degree of cervical squamous carcinoma

Xing Meng<sup>1,2</sup>, Shifeng Tian<sup>1</sup>, Changjun Ma<sup>1</sup>, Liangjie Lin<sup>3</sup>,  
Xiaoxiao Zhang<sup>3</sup>, Jiazheng Wang<sup>3</sup>, Qingwei Song<sup>1</sup>  
and Ai Lian Liu<sup>1\*</sup>

<sup>1</sup>First Affiliated Hospital, Dalian Medical University, Dalian, Liaoning, China, <sup>2</sup>Radiology Department, Dalian Women and Children's Medical Group, Dalian, Liaoning, China, <sup>3</sup>Radiology Department, Philips (China), Beijing, China

**Background:** To investigate the value of amide proton transfer weighted (APTw) imaging combined with modified Dixon fat quantification (mDixon-Quant) imaging in determining the degree of differentiation of cervical squamous carcinoma (CSC) against histopathologic.

**Methods:** Magnetic resonance imaging (MRI) data were collected from 52 CSC patients. According to histopathologic results, patients were divided into the poorly differentiated group (37 cases) and the well/moderately differentiated group (15 cases). The APTw value by APTw imaging and the fat fraction (FF) and transverse relaxation rate  $R_2^*$  values by mDixon-Quant were independently measured by two radiologists. Intra-class correlation coefficients (ICCs) were used to test the consistency of APTw, FF, and  $R_2^*$  values measured by the two observers. The Mann-Whitney U test was used to analyze the difference in each parameter between the two groups. Logistic regression analysis was used to assess the association between the degree of differentiation on histopathology and imaging parameters by APTw and mDixon Quant. The ROC curve was used to evaluate the diagnostic efficacy of various parameters and their combination in distinguishing the degree of CSC differentiation on histopathology. The DeLong test was used to access the differences among the area under the ROC curves (AUCs). The Pearson correlation coefficient was used to evaluate the correlation between APTw and mDixon-Quant imaging parameters.

**Results:** The APTw means were  $2.95 \pm 0.78\%$  and  $2.05 (1.85, 2.65)\%$  in the poorly and well/moderately differentiated groups, respectively. The  $R_2^*$  values were  $26.62 (21.99, 33.31)/s$  and  $22.93 \pm 6.09/s$  in the poorly and well/moderately differentiated groups, respectively ( $P < 0.05$ ). The AUCs of APTw,  $R_2^*$ , and their combination were 0.762, 0.686, and 0.843, respectively. The Delong test suggested statistical significance between  $R_2^*$  and the combination of APTw and  $R_2^*$ .  $R_2^*$  values showed a significant correlation with APTw values in the poorly differentiated group.

**Conclusions:** APTw combined with mDixon-Quant can be used to efficiently distinguish the differentiation degrees of CSC diagnosed on histopathology.

KEYWORDS

magnetic resonance imaging, amide proton transfer weighted, modified Dixon-Quant, transverse relaxation rate, cervical squamous carcinoma

## 1 Introduction

Cervical cancer is a malignant tumor that threatens the health and life of women worldwide. According to the global cancer data in 2018, cervical cancer ranks fourth in the incidence and mortality of female patients with malignant tumors (1). Cervical squamous carcinoma (CSC) is a common pathologic type of cervical tumors. The degree of tumor differentiation is a prognostic factor of CSC, especially during the early stages of the disease. The higher the pathologic tumor grade, the worse the degree of differentiation, the easier for the tumor to locally invade and form distant metastases, the higher the recurrence rate, the worse the prognosis, and the lower the survival rate (2–5). Histopathologic tumor types, the degree of tumor differentiation, and the stages of cervical cancer are key factors when choosing a treatment plan and assessing prognosis. Therefore, accurately determining the degree of cervical cancer differentiation on histopathology is critical.

Cervical biopsy is a common diagnostic method for cervical cancer, but it is an invasive method and not suitable for patients with cervical or vaginal stenosis. Besides, the accuracy of cervical biopsy can be affected by human factors, such as sample size, location of sampling, etc. MRI, as a noninvasive examination method, plays an important role in evaluation of the staging and degree of differentiation of cervical cancer. The modified Dixon fat quantification (mDixon-Quant) technique is a water-fat separation technology that enables semutaneous mapping of proton density fat fraction and transverse relaxation rate  $R_2^* = 1/T_2^*$  (6), thus reflecting the fat contents and iron deposition in tissues. mDixon-Quant has been used to diagnose spinal lesions (7), detect liver lesions (8, 9), measure testicular and epididymal fat content (10), and quantitatively analyze muscle fat content (11).

Amide proton transfer weighted (APTw) imaging is a subtype of chemical exchange saturation transfer imaging, which use off-resonance saturation pulses to detect free protein and polypeptide molecules in cell cytoplasm without using an exogenous contrast agent (12). It has been widely explored for clinical applications, such as evaluating glioma grades (13), diagnosing and estimating the severity of Parkinson's disease (14), differentiating benign and malignant tumors of the head and neck (15) and breast (16), diagnosing prostate cancer and performing risk assessments (17),

evaluating the prognostic factors of rectal adenocarcinoma (18), and predicting the histologic grade of hepatocellular carcinoma (19).

To the best of our knowledge, the use of quantitative APTw and mDixon-Quant imaging to evaluate the degree of CSC differentiation compared with histopathology has not been reported. This study explored the value of APTw and mDixon-Quant in evaluating the degree of CSC differentiation and thus provides valuable information for preoperative diagnoses and treatments.

## 2 Materials and methods

### 2.1 Study population

The patients with cervical cancer who underwent MRI examinations from May 2019 to February 2022 were retrospectively identified from the database. We included patients who meet the criteria of 1) a tumor size > 1 cm in diameter; 2) had not received radiotherapy, chemotherapy, or any other treatment. Pelvic 3.0T MRI examinations were performed before the surgeries. The exclusion criteria were 1) incomplete pathologic information or lack of grading-related information, and 2) poor image quality. Finally, 52 cases of CSC were included in this study, which was divided into a poorly differentiated group (37 cases) and a well/moderately differentiated group (15 cases) based on the pathologic results. The CSC patients in current study were commonly associated with abnormal vaginal bleeding, while the clinical manifestations in patients with poorly differentiated and well/moderately tumors were similar (Table 1).

### 2.2 Imaging protocol

MR scans, including  $T_2$  weighted imaging ( $T_2$ WI), APTw, and mDixon-Quant, were performed on a 3.0T MRI scanner (Ingenia CX, Philips Healthcare, Best, the Netherlands) equipped with a 32-channel abdominal coil. MR scan parameters are listed in Table 2.

APTw imaging used a 3D fast spin-echo sequence. Signals were acquired with the radiofrequency saturation pulses applied at frequencies of  $\pm 2.7$ ,  $\pm 3.5$ , and  $\pm 4.3$  ppm using the B1 intensity (rms) of 2  $\mu$ T and a duration of 2 seconds for fitting of the Z-spectrum (with the water frequency defined as 0 ppm). The reference scan is obtained by setting the saturation frequency to -1540 ppm. The data from three different echo times were collected at the saturation frequency of +3.5 ppm to generate the B0 map for the B0 correction of the Z-spectrum in each image voxel. The APTw value was obtained by calculating the asymmetry of the traditional

**Abbreviations:** APTw, amide proton transfer weighted; mDixon-Quant, modified Dixon fat quantification; CSC, cervical squamous carcinoma; MRI, magnetic resonance imaging; ICC, intra-class correlation coefficient; ROC, receiver operating characteristic; AUC, area under the ROC curve;  $T_2$ WI,  $T_2$  weighted imaging; ROI, region of interest.

TABLE 1 Comparison of clinical data of patients in the poorly differentiated and well/moderately differentiated groups.

		Poorly differentiated group (n=37)	Well/moderately differentiated group (n=15)	t/ $\chi^2$ values	P-value
Age (yr)		53.9 ± 11.1	55.2 ± 7.0	-0.488*	0.629
Menopause status	pre	14 (37.8%)	4 (26.7%)	0.588	0.443
	post	23 (62.2%)	11 (73.3%)		
Vaginal bleeding	with	27 (73.0%)	10 (66.7%)	0.207	0.907
	without	10 (27.0%)	5 (33.3%)		

\*: t values.

magnetization transfer effect at 3.5 ppm on both sides of the water signal (20).

mDixon-Quant uses a 3D gradient echo sequence. In this study, it measured images at the 6 echo times (TEs) of 1.11, 1.81, 2.61, 3.41, 4.21, and 5.01 ms, respectively. The post-processing of both APTw and mDixon-Quant imaging was performed on the MR console after data collection. After phase correction, accurate fat quantification was achieved with a seven-peak spectral fat model that enabled T2\* corrections (21). The proton density fat fraction (FF) map was computed as the ratio of the fat signal over the sum of fat and water signals.

## 2.3 Image processing and data analysis

Images were uploaded to the IntelliSpace Portal (ISP v9.0, Philips Healthcare) workstation for quantitative measurements. Regions of interest (ROIs) were drawn independently by two radiologists (both with 10 years of diagnostic experience in abdominal radiology), who were blinded to the clinical information and histopathologic results. The ROIs of lesions on the APTw images were delineated on the slice showing the largest lesion diameter with reference to the T<sub>2</sub>WI images (Figure 1). The ROIs aimed to encompass the entire tumor, excluding regions such as cystic changes, hemorrhage, necrotic areas, and tumor boundaries to avoid partial volume effects. ROIs of the mDixon-Quant images were drawn to match as closely as possible the position of the lesion drawn on the APTw images.

## 2.4 Statistical analysis

All statistical analyses were conducted with SPSS 26.0 software unless otherwise specified. Intra-class correlation coefficients (ICCs)

were used to test the consistency of the APTw, FF, and R<sub>2</sub>\* values determined by the two observers. The ICC < 0.40; 0.40 ≤ ICC < 0.75; and ICC ≥ 0.75 were regarded as poor, medium, and good consistency, respectively. Mean values by the two observers were used for subsequent statistical analysis. Continuous variables were compared between the poorly differentiated and well/moderately differentiated groups with the independent samples *t* test or Mann-Whitney U test, and categorical variables were compared with the chi-square test or Fisher's exact test. Kolmogorov Smirnov test was used to test the normality of the continuous variables. Logistic regression was used to assess the association between the degree of differentiation on histopathology specimens and imaging parameters by APTw and mDixon-Quant. The receiver operator characteristic (ROC) curve was used to evaluate the diagnostic efficacy of different parameters. From the ROC curves, the area under the curve (AUC), threshold, sensitivity and specificity were obtained. The difference in AUCs between models was detected with the DeLong test using MedCalc v15.2.2 software (MedCalc Software, Ostend, Belgium). The Pearson correlation coefficient was used to evaluate correlations between the APTw and mDixon-Quant parameters. A P-value < 0.05 was considered statistically significant.

## 3 Results

### 3.1 Comparison of the clinical data between the poorly differentiated and well/moderately differentiated groups

Age, menopause status, and vaginal bleeding of the patients in the poorly differentiated and well/moderately differentiated groups are presented in Table 1. There was no significant difference in clinical indices between the two groups (P > 0.05).

TABLE 2 T<sub>2</sub>WI, APTw, and mDixon-Quant scan parameters.

	TA (min/sec)	NSA	TR (ms)	FOV (mm <sup>2</sup> )	Pixel size (mm <sup>2</sup> )	Slice thickness/gap (mm)
T <sub>2</sub> WI	59s	1	3672/95	240×240	0.7×0.7	4.0/1.0
APTw	4 min 45s	1	5174/7.8	130×130	2.0×2.0	7.0/0.0
mDixon-Quant	15s	1	6	375×375	2.3×1.8	5.0/-2.5

TA, acquisition time; NSA, number of signal averages; TR, repetition time; FOV, field of view; T<sub>2</sub>WI, T<sub>2</sub> weighted imaging; APTw, amide proton transfer weighted.

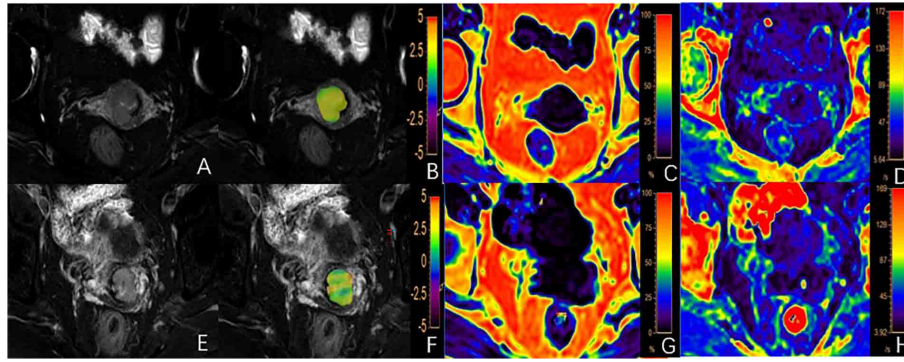


FIGURE 1

(A-D) A 62-year-old patient with a poorly differentiated cervical squamous carcinoma (CSC): (A) T<sub>2</sub>WI image, (B) fused APTw and T<sub>2</sub>WI image with the APTw value for the lesion of 2.45%; (C, D) FF and R<sub>2</sub><sup>\*</sup> images with FF and R<sub>2</sub><sup>\*</sup> values for the lesion of 2.69% and 19.62/s, respectively; (E-H) A 56-year-old patient with well/moderately differentiated CSC: (E) T<sub>2</sub>WI image; (F) fused APTw and T<sub>2</sub>WI image with an APTw value for the lesion of 2.05%; (G, H) The FF and R<sub>2</sub><sup>\*</sup> images with FF and R<sub>2</sub><sup>\*</sup> values for the lesion of 1.04% and 19.51/s, respectively.

### 3.2 Data consistency between the two observers

The intra-class agreements between the two observers were good for the APTw, FF, and R<sub>2</sub><sup>\*</sup> values in both groups (all ICC ≥ 0.75, Table 3).

### 3.3 Comparison of parameters between the two groups

The APTw and R<sub>2</sub><sup>\*</sup> values of the poorly differentiated group were significantly higher than those of the well/moderately differentiated group ( $P < 0.05$ , Table 4). There were no statistically significant difference in FF measurements between the two groups ( $P > 0.05$ ). Representative images from a patient in the poorly differentiated group and one in the well/moderately differentiated group are presented in Figure 1.

### 3.4 Diagnostic performance of each parameter and their combination for diagnostic efficacy

The APTw and R<sub>2</sub><sup>\*</sup> values with significant difference between the two histopathologic groups were included in the ROC test (Table 5).

The AUCs of APTw and R<sub>2</sub><sup>\*</sup> values for diagnosis of poorly and well/moderately differentiation of CSC were 0.762 and 0.686, respectively. The combined R<sub>2</sub><sup>\*</sup> value significantly improve the diagnostic performance (AUC = 0.843). The result of the Delong test suggested a statistical significance between AUCs by R<sub>2</sub><sup>\*</sup> and combined APTw + R<sub>2</sub><sup>\*</sup> values (Table 6).

R<sub>2</sub><sup>\*</sup> values were significantly correlated with APTw values in the poorly differentiated group ( $P < 0.05$ ) (Table 7).

## 4 Discussion

APT<sub>w</sub> and mDixon-Quant imaging were evaluated in this study for discrimination of the differentiation degree of CSC by histopathology. The APT<sub>w</sub> and R<sub>2</sub><sup>\*</sup> values of the poorly differentiated group were significantly higher than those of the well/moderately differentiated group. And the combination of APT<sub>w</sub> and R<sub>2</sub><sup>\*</sup> values showed a high diagnostic efficacy in discrimination of CSC with different differentiation degrees.

A previous study on cervical cancer showed that moderately and poorly differentiated tumors were more common than well-differentiated tumors (22). In this study, the sample size of the poorly differentiated group was also much larger than that of the well/moderately differentiated group. The treatment scheme of CSC is highly based on the degree of histopathologic differentiation.

TABLE 3 APT<sub>w</sub>, FF, and R<sub>2</sub><sup>\*</sup> measurement consistency between two observers.

		Observer 1	Observer 2	ICC
APT <sub>w</sub> (%)	poorly differentiated group	2.95 ± 0.79	2.94 ± 0.80	0.959
	well/moderately differentiated group	2.10(1.80, 2.70)	2.20(1.70, 2.40)	0.963
FF (%)	poorly differentiated group	2.17(1.17, 3.38)	2.32 ± 1.20	0.899
	well/moderately differentiated group	2.42 ± 0.84	2.32 ± 0.88	0.813
R <sub>2</sub> <sup>*</sup> (/s)	poorly differentiated group	28.09 ± 7.90	27.25 ± 6.99	0.921
	well/moderately differentiated group	22.13 ± 5.81	23.72 ± 6.73	0.936

ICC, intraclass correlation coefficient; APT<sub>w</sub>, amide proton transfer weighted imaging; FF, fat fraction.

TABLE 4 Comparison of APTw and mDixon-Quant parameters between the two groups.

	poorly differentiated group (n=37)	well/moderately differentiated group (n=15)	z values	P value
APT <sub>w</sub> (%)	2.95 ± 0.78	2.05 (1.85, 2.65)	-2.940	0.003
FF (%)	2.13 (1.32, 3.09)	2.37 ± 0.79	-0.495	0.621
R <sub>2</sub> <sup>*</sup> (/s)	26.62 (21.99, 33.31)	22.93 ± 6.09	-2.090	0.037

APT<sub>w</sub>, amide proton transfer weighted imaging; FF, fat fraction.

TABLE 5 Diagnostic efficacy of each parameter.

	AUC	Sensitivity (%)	Specificity (%)	Threshold value
APT <sub>w</sub>	0.762	81.1	73.3	2.25%
R <sub>2</sub> <sup>*</sup>	0.686	51.4	80	26.53(/s)
APT <sub>w</sub> + R <sub>2</sub> <sup>*</sup>	0.843	67.6	93.3	—

AUC, area under the curve; APT<sub>w</sub>, amide proton transfer weighted imaging; APT<sub>w</sub> + R<sub>2</sub><sup>\*</sup>, APT<sub>w</sub> combined with R<sub>2</sub><sup>\*</sup>.

TABLE 6 Receiver operating characteristic curve paired with the Delong test.

	Z-values	P-values
APT <sub>w</sub> vs. R <sub>2</sub> <sup>*</sup>	0.629	0.5294
APT <sub>w</sub> vs. APT <sub>w</sub> + R <sub>2</sub> <sup>*</sup>	1.189	0.2345
R <sub>2</sub> <sup>*</sup> vs. APT <sub>w</sub> + R <sub>2</sub> <sup>*</sup>	2.284	0.0224

APT<sub>w</sub>, amide proton transfer weighted imaging; APT<sub>w</sub> + R<sub>2</sub><sup>\*</sup>, APT<sub>w</sub> combined with R<sub>2</sub><sup>\*</sup>.

TABLE 7 Correlations between the APTw and mDixon-Quant parameters.

	Poorly differentiated group		Well/moderately differentiated group	
	r values	P-values	r values	P-values
FF	0.089	0.599	0.074	0.793
R <sub>2</sub> <sup>*</sup>	-0.394	0.016	-0.188	0.503

FF, fat fraction; APT<sub>w</sub>, amide proton transfer weighted imaging.

Compared with well-differentiated CSC, poorly differentiated CSC has a poorer prognosis and shorter survival time. In a study by McCluggage et al, the total survival time of patients with well, moderately, and poorly differentiated CSC was 143.4 months, 124.2 months, and 86.1 months, respectively (23).

Early cervical cancer is primarily asymptomatic and may be accompanied by watery vaginal secretions, post-coital bleeding, or intermittent punctate bleeding. Usually, these early symptoms are not noticed by patients, and the disease often becomes more serious with delays in treatment. In our study, older postmenopausal patients with abnormal vaginal bleeding were common; however, the clinical manifestations of patients in the poorly differentiated and well/moderately differentiated CSC groups were similar.

The R<sub>2</sub><sup>\*</sup> value can be non-invasively determined by the mDixon Quant with elimination of the interference from fat signals. İdilman et al. (24) evaluated iron concentrations with R<sub>2</sub><sup>\*</sup> values in fat-rich organs, such as the liver, pancreas, and bone marrow, and found that the iron content in organs was underestimated without fat suppression and significantly improved after fat suppression. In this study, the R<sub>2</sub><sup>\*</sup> values of poorly differentiated tumors were significantly higher than those of the well/moderately differentiated tumors. As we know, R<sub>2</sub><sup>\*</sup> is sensitive to local magnetic field inhomogeneity (25). When the paramagnetic material of blood metabolites including deoxyhemoglobin and hemosiderin produce local inhomogeneous magnetic field, the R<sub>2</sub><sup>\*</sup> value increases (26). In cervical cancer, the growth and metabolism in poorly differentiated tumor cells can be more vigorous and tissue oxygen consumption increases, resulting in a state of hypoxia and a need for more nutrients, such as sugar, protein, and oxygen (27). An increase in the concentration of paramagnetic material ensues with an increase in the R<sub>2</sub><sup>\*</sup> value.

The results of this study showed that the APT<sub>w</sub> values of poorly differentiated CSC were significantly higher than those of well/moderately differentiated CSC. Liu et al. showed that tumor cell densities and tumor pathologic grades positively correlated in patients with uterine cervical cancer (28). In our study, the poorly differentiated CSC were commonly with a higher degree of malignancy compared with well/moderately differentiated CSC. Therefore, poorly differentiated CSC cells should have more active proliferation and higher cell densities than well/moderately differentiated CSC cells, allowing additional free proteins and polypeptides to be synthesized. APT<sub>w</sub> signal reflects free protein and polypeptide concentrations in tissues, and can be affected by the heterogeneity and composition of tumors (16). Thus, APT<sub>w</sub> values in poorly differentiated cancer types are higher than those in well/moderately differentiated cancer types, as has been reported previously (29–31).

Combination of APT<sub>w</sub> and R<sub>2</sub><sup>\*</sup> image analysis can provide information about cell proliferation by measuring the changes in protein concentrations and iron content in tumor microenvironments, and thus showed improved diagnosis between poorly and well/moderately CSC. APT<sub>w</sub> and R<sub>2</sub><sup>\*</sup> values were significantly correlated in poorly differentiated CSC cases but not in the well/moderately differentiated CSC cases. These observations need verification with research on larger samples.

This study has some limitations. First, the sample size is relatively small, and thus the well- and moderately- differentiated CSC were combined into one group. As a result, the difference between the two degrees of differentiation were not fully compared. Also limited by sample size, microsatellite instability and other immunohistochemical indexes have not been studied in detail. Further studies with increased sample sizes are expected to exploit the capacity of APT<sub>w</sub> to

differentiate other prognostic factors and predict cervical cancer prognosis.

## 5 Conclusions

APTw and mDixon-Quant imaging were investigated for clinical non-invasive evaluation of CSC differentiation. APTw combined with  $R_2^*$  values showed a high efficacy in discriminating poorly from well/moderately differentiated CSC, and may help the treatment design and prognosis prediction of CSC.

## Data availability statement

The raw data supporting the conclusions of this article will be made available by the authors, without undue reservation.

## Ethics statement

The studies involving human participants were reviewed and approved by The First Affiliated Hospital of Dalian Medical University. Written informed consent for participation was not required for this study in accordance with the national legislation and the institutional requirements.

## References

- Bray F, Ferlay J, Soerjomataram I, Siegel RL, Torre LA, Jemal A. Global cancer statistics 2018: GLOBOCAN estimates of incidence and mortality worldwide for 36 cancers in 185 countries [published correction appears in *CA Cancer J Clin* (2018) 68(6):394–424. doi: 10.3322/caac.21492
- Wu C, Ma C, Yuan J, Zhou P. Exploration of potential therapeutic and prognostic value of CXC chemokines in cervical squamous cell carcinoma and endocervical adenocarcinoma based on bioinformatics analysis. *Math Biosci Eng* (2021) 18(6):8201–22. doi: 10.3934/mbe.2021407
- Zhang H, Cheng C, Gao R, Yan Z, Zhu Z, Yang B, et al. Rapid identification of cervical adenocarcinoma and cervical squamous cell carcinoma tissue based on raman spectroscopy combined with multiple machine learning algorithms. *Photodiagnosis Photodyn Ther* (2021) 33:102104. doi: 10.1016/j.pdpdt.2020.102104
- Matsuo K, Mandelbaum RS, Machida H, Purushotham S, Grubbs BH, Roman LD, et al. Association of tumor differentiation grade and survival of women with squamous cell carcinoma of the uterine cervix. *J Gynecol Oncol* (2018) 29(6):e91. doi: 10.3802/jgo.2018.29.e91
- Hou M, Song K, Ren J, Wang K, Guo J, Niu Y, et al. Comparative analysis of the value of amide proton transfer-weighted imaging and diffusion kurtosis imaging in evaluating the histological grade of cervical squamous carcinoma. *BMC Cancer* (2022) 22(1):87. doi: 10.1186/s12885-022-09205-z
- Yoo H, Lee JM, Yoon JH, Kang HJ, Lee SM, Yang HK, et al. T2\* mapping from multi-echo Dixon sequence on gadoteric acid-enhanced magnetic resonance imaging for the hepatic fat quantification: Can it be used for hepatic function assessment? *Korean J Radiol* (2017) 18(4):682–90. doi: 10.3348/kjr.2017.18.4.682
- Zhang Y, Zhou Z, Wang C, Cheng X, Wang L, Duanmu Y, et al. Reliability of measuring the fat content of the lumbar vertebral marrow and paraspinous muscles using MRI mDIXON-quant sequence. *Diagn Interv Radiol* (2018) 24(5):302–7. doi: 10.5152/dir.2018.17323
- Zhang Y, Wang C, Duanmu Y, Zhang C, Zhao W, Wang L, et al. Comparison of CT and magnetic resonance mDIXON-quant sequence in the diagnosis of mild hepatic steatosis. *Br J Radiol* (2018) 91(1091):20170587. doi: 10.1259/bjr.20170587
- Zhou N, Hu A, Shi Z, Wang X, Zhu Q, Zhou Q, et al. Inter-observer agreement of computed tomography and magnetic resonance imaging on gross tumor volume delineation of intrahepatic cholangiocarcinoma: An initial study. *Quant Imaging Med Surg* (2021) 11(2):579–85. doi: 10.21037/qims-19-1093

## Author contributions

XM and AL conceived of the presented idea. XM and CM performed the measurements. ST were supervised the work. XM and LL processed the experimental data, performed the analysis. XM drafted the manuscript, and LL, XZ and JW aided in working on the manuscript. QS carries out image scanning. All authors discussed the results and contributed to the final manuscript. All authors contributed to the article and approved the submitted version.

## Conflict of interest

Authors LL, XZ, and JW were employed by Philips China.

The remaining authors declare that the research was conducted in the absence of any commercial or financial relationships that could be construed as a potential conflict of interest.

## Publisher's note

All claims expressed in this article are solely those of the authors and do not necessarily represent those of their affiliated organizations, or those of the publisher, the editors and the reviewers. Any product that may be evaluated in this article, or claim that may be made by its manufacturer, is not guaranteed or endorsed by the publisher.

- Guo RM, Zhao RZ, Zhang J, Yang F, Wen HQ, Wang J, et al. Quantification of fat deposition in the testis and epididymis using mDIXON quant sequence: correlation with age and ejaculation. *Abdom Radiol (NY)* (2019) 44(4):1528–34. doi: 10.1007/s00261-018-1826-3
- Duijnsveld BJ, Henseler JF, Reijnierse M, Fiocco M, Kan HE, Nelissen RG. Quantitative Dixon MRI sequences to relate muscle atrophy and fatty degeneration with range of motion and muscle force in brachial plexus injury. *Magn Reson Imaging* (2017) 36:98–104. doi: 10.1016/j.mri.2016.10.020
- He YL, Li Y, Lin CY, Qi YF, Wang X, Zhou HL, et al. Three-dimensional turbo-spin-echo amide proton transfer-weighted mri for cervical cancer: A preliminary study. *J Magn Reson Imaging* (2019) 50(4):1318–25. doi: 10.1002/jmri.26710
- Bai Y, Lin Y, Zhang W, Kong L, Wang L, Zuo P, et al. Noninvasive amide proton transfer magnetic resonance imaging in evaluating the grading and cellularity of gliomas. *Oncotarget* (2017) 8(4):5834–42. doi: 10.18632/oncotarget.13970
- Li C, Chen M, Zhao X, Wang R, Chen H, Su W, et al. Chemical exchange saturation transfer MRI signal loss of the SubstantiaNigra as an imaging biomarker to evaluate the diagnosis and severity of parkinson's disease. *Front Neurosci* (2017) 11:489. doi: 10.3389/fnins.2017.00489
- Law BKH, King AD, Ai QY, Poon DMC, Chen W, Bhatia KS, et al. Head and neck tumors: Amide proton transfer MRI. *Radiology* (2018) 288(3):782–90. doi: 10.1148/radiol.2018171528
- Meng N, Wang XJ, Sun J, Huang L, Wang Z, Wang KY, et al. Comparative study of amide proton transfer-weighted imaging and intravoxel incoherent motion imaging in breast cancer diagnosis and evaluation. *J Magn Reson Imaging* (2020) 52(4):1175–86. doi: 10.1002/jmri.27190
- Yin H, Wang D, Yan R, Jin X, Hu Y, Zhai Z, et al. Comparison of diffusion kurtosis imaging and amide proton transfer imaging in the diagnosis and risk assessment of prostate cancer. *Front Oncol* (2021) 11:640906. doi: 10.3389/fonc.2021.640906
- Chen W, Li L, Yan Z, Hu S, Feng J, Liu G, et al. Three-dimension amide proton transfer MRI of rectal adenocarcinoma: Correlation with pathologic prognostic factors and comparison with diffusion kurtosis imaging. *Eur Radiol* (2021) 31(5):3286–96. doi: 10.1007/s00330-020-07397-1
- Wu B, Jia F, Li X, Li L, Wang K, Han D. Comparative study of amide proton transfer imaging and intravoxel incoherent motion imaging for predicting histologic grade of hepatocellular carcinoma. *Front Oncol* (2020) 10:562049. doi: 10.3389/fonc.2020.562049

20. Zhou J, Payen JF, Wilson DA, Traystman RJ, van Zijl PC. Using the amide proton signals of intracellular proteins and peptides to detect pH effects in MRI. *Nat Med* (2003) 9(8):1085–90. doi: 10.1038/nm907
21. Lohöfer FK, Kaissis GA, Müller-Leisse C, Franz D, Katemann C, Hock A, et al. Acceleration of chemical shift encoding-based water fat MRI for liver proton density fat fraction and T2\* mapping using compressed sensing. *PLoS One* (2019) 14(11):e0224988. doi: 10.1371/journal.pone.0224988
22. Zimmermann F, Korzowski A, Breitling J, Meissner JE, Schuenke P, Loi L, et al. A novel normalization for amide proton transfer CEST MRI to correct for fat signal-induced artifacts: application to human breast cancer imaging. *Magn Reson Med* (2020) 83(3):920–34. doi: 10.1002/mrm.27983
23. McCluggage WG. Towards developing a meaningful grading system for cervical squamous cell carcinoma. *J Pathol Clin Res* (2018) 4(2):81–5. doi: 10.1002/cjp2.98
24. İdilman İS, Gümrük F, Haliloğlu M, Karçaaltınçaba M. The feasibility of magnetic resonance imaging for quantification of liver, pancreas, spleen, vertebral bone marrow, and renal cortex R2\* and proton density fat fraction in transfusion-related iron overload. *Turk J Haematol* (2016) 33(1):21–7. doi: 10.4274/tjh.2015.0142
25. Karlsson M, Ekstedt M, Dahlström N, Forsgren MF, Ignatova S, Norén B, et al. Liver R2\* is affected by both iron and fat: A dual biopsy-validated study of chronic liver disease. *J Magn Reson Imaging* (2019) 50(1):325–33. doi: 10.1002/jmri.26601
26. Han X, Sun M, Wang M, Fan R, Chen D, Xie L, et al. The enhanced T2 star weighted angiography (ESWAN) value for differentiating borderline from malignant epithelial ovarian tumors. *Eur J Radiol* (2019) 118:187–93. doi: 10.1016/j.ejrad.2019.07.011
27. Yang X. The role of metabolic syndrome in endometrial cancer: A review. *Front Oncol* (2019) 9:744. doi: 10.3389/fonc.2019.00744
28. Liu Y, Ye Z, Sun H, Bai R. Clinical application of diffusion-weighted magnetic resonance imaging in uterine cervical cancer. *Int J Gynecol Cancer* (2015) 25(6):1073–8. doi: 10.1097/IGC.0000000000000472
29. Li B, Sun H, Zhang S, Wang X, Guo Q. Amide proton transfer imaging to evaluate the grading of squamous cell carcinoma of the cervix: A comparative study using 18 f FDG PET. *J Magn Reson Imaging* (2019) 50(1):261–8. doi: 10.1002/jmri.26572
30. Li B, Sun H, Zhang S, Wang X, Guo Q. The utility of APT and IVIM in the diagnosis and differentiation of squamous cell carcinoma of the cervix: A pilot study. *Magn Reson Imaging* (2019) 63:105–13. doi: 10.1016/j.mri.2019.08.020
31. Meng N, Wang J, Sun J, Liu W, Wang X, Yan M, et al. Using amide proton transfer to identify cervical squamous carcinoma/adenocarcinoma and evaluate its differentiation grade. *Magn Reson Imaging* (2019) 61:9–15. doi: 10.1016/j.mri.2019.05.005